

ANALYSIS OF THE DISCRETE REPRESENTATION METHOD TO COMPUTE ECHO RESPONSES FROM CIRCULAR CONCAVITY DEFECT

Paulo Orestes Formigoni, paulo.formigoni@poli.usp.br

Orlando Cirullo Filho, cirullinux@gmail.com

School of Engineering at University of São Paulo, Department of Mechatronics Engineering
Av. Prof. Mello Moraes, 2231, CEP 05508-900, São Paulo, Brazil

Julio C. Adamowski, jcadamow@usp.br

School of Engineering at University of São Paulo, Department of Mechatronics Engineering
Av. Prof. Mello Moraes, 2231, CEP 05508-900, São Paulo, Brazil

Flávio Buiochi, fbuiochi@usp.br

School of Engineering at University of São Paulo, Department of Mechatronics Engineering
Av. Prof. Mello Moraes, 2231, CEP 05508-900, São Paulo, Brazil

Abstract. *This work analyzes the discrete representation method to compute the acoustic wave generated by ultrasonic transducers, its interaction with a concave circular defect on a plane surface, and the echoes received by the transducer. The method is divided into three computational parts. As first step, the velocity potential impulse response is determined at the interface using the Rayleigh integral. In a second step, the reflected field is calculated considering that every elementary portion of the interface radiates a hemispherical wave (Huygens principle). Finally, the acoustic pressure over the surface of the receiver is determined by a temporal convolution between the excitation signal and the spatial reflected velocity potential impulse response. The accuracy and the temporal computational cost depend on the spatial sampling of the aperture and interface, and on the time sampling of the transmitted signals. The aim of the work is to determine a compromise between the accuracy and the computational time, having the temporal sampling of the transmitted signal and the spatial sampling of the aperture and interface with the defect as variables.*

Keywords *Acoustic field, ultrasound, simulation, impulsive response, pulse-echo response*

1. INTRODUCTION

Modeling of the echo responses caused by circular type defects is an important tool for nondestructive testing using broadband ultrasonic transducer. For instance, the preventive maintenance of pipelines requires finding pitting corrosion defects, which can be done by using pulse-echo mode. It tries to get as much information as possible from the existing defect. However, identifying the defect geometry is not an easy task in realistic situation. Modeling of echo responses from circular concavity defects allows both recognizing the variability of echoes as corrosion grows and selecting the optimal broadband ultrasonic transducer, such that the axial and lateral resolutions are improved. In this work the discrete representation method is described.

The discrete representation method (Piwakowski et al, 1989 and 1999) computationally predicts the echo response of arbitrary geometry defects. It uses a model that calculates the longitudinal wave evolution caused by interfaces (Buiochi et al, 2004), based on the impulse response method (Stepanishen, 1971). Both methods are suitable for all field regions and can be performed for any excitation wavelength.

The validation of the wave propagation models implemented in the ongoing paper requires experimental corroboration, which is done by using broadband ultrasonic transducers operating in pulse-echo mode, and a circular concavity defect embedded in planar reflector. A 19-mm-diam 2.25-MHz transducer and a 6.3-mm-diam, a 10-mm-diam and 19-mm-diam 5-MHz transducers were used. The errors between experimental and theoretical curves were analyzed by varying the aperture and the reflector surface discretization, and the processing times were studied.

2. DISCRETE REPRESENTATION METHOD

The computational method solution proposed by Buiochi et al. (Buiochi et al, 2004), which calculates the acoustic field through interfaces, is easily used to calculate the pulse-echo responses using the same theoretical concepts. The proposed solution is an approximated method that operates by dividing the aperture and the interface with a defect into elementary areas, as shown in Fig. 1. The radiated and reflected acoustic fields result from the superposition of the hemispherical waves generated, respectively (Harris, 1981, Robinson et al, 1974 and Weight, 1971), from each emitter and interface elementary areas. In this work, as the defect is slightly concave, and the emitter/receiver aperture and the planar interface are parallels, the mode conversion at the reflector surfaces was not considered.

Considering an aperture with arbitrary radiating surface S_A embedded in an infinite rigid baffle, the velocity potential impulse response on each point P_i at the interface due to the aperture radiation is given by:

$$h^l(\vec{r}_i, t) = \int_{S_A} \frac{\delta(t - r_{ai}/c)}{2\pi r_{ai}} dS_a \quad (1)$$

where r_{ai} is the distance from each radiating elementary area dS_a to the point P_i .

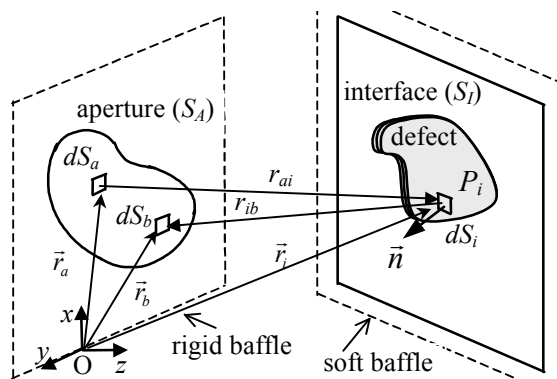


Figure 1. Arbitrary geometry used to determine the pulse-echo mode response using discrete representation method.

Assume that the interface with defect is embedded in an infinite soft baffle and that it is large enough to intercept the main incident energy of the acoustic beam. The whole-extended interface and the defect are approximated by elementary areas dS_i . In each of the receptor aperture elementary areas dS_b , the velocity potential impulse response is calculated from the impulse response obtained at the interface by:

$$h^A(\vec{r}_b, t) = \frac{1}{2\pi c} \int_{S_I} \frac{\cos \theta_{ib}}{r_{ib}} \frac{\partial}{\partial t} h^I(\vec{r}_i, t - \frac{r_{ib}}{c}) dS_i \quad (2)$$

where S_I is the surface of the interface with the defect, r_{ib} is the distance from the elementary area dS_i located at \vec{r}_i to the point located at \vec{r}_b in the aperture, and θ_{ib} is the angle between the normal vector at P_i and the vector \vec{r}_{ib} .

Finally, the spatial acoustic pressure $\langle p(\vec{r}_b, t) \rangle$ over the surface of the finite receiver is calculated by the following temporal convolution:

$$\langle p(\vec{r}_b, t) \rangle = \rho \frac{\partial v(t)}{\partial t} * \langle h(\vec{r}_b, t) \rangle \quad (3)$$

where $v(t)$ is the excitation signal, ρ is the density of the propagation medium, and $\langle h(\vec{r}_b, t) \rangle$ is defined by:

$$\langle h(\vec{r}_b, t) \rangle = \int_{S_A} h^A(\vec{r}_b, t) dS_b \quad (4)$$

3. RESULTS

Echo responses were obtained from a circular concavity defect to test the validity of the discrete representation method. Fig. 2 shows the geometry of such defect, which was produced on the plane surface of an aluminum solid sample. It also shows the seven positions used to simulate the transducers displacements. Setting the center of the defect as zero (position 1), the positions 1 through 7 are displaced $x_{off} = 0, 5, 10, 15, 20, 25$ and 30 mm, respectively. The transducers were placed 10 mm from the plane surface of the sample and were excited with short pulses by a pulser/receiver Panametrics 5072PR, Oscilloscope DSO6052-A of 500MHz (Agilent Technologies). All measurements were carried out in water ($\rho=1000$ kg/m³, $c=1480$ m/s), using four transducers: 19-mm-diam 2.25-MHz transducer 25MHz (V305-512968, Panametrics, USA), 6.3-mm-diam 5-MHz transducer (0043V3 alpha, Aeroteck, USA), a 10-mm-diam 5-MHz transducer (USP-EPUSP, Brazil), and 19-mm-diam 5-MHz transducer (008700 alpha, Aeroteck, USA).

Simulations were performed in Matlab using the same parameters described above for the experiments in order to allow the comparison of echo responses arising from the defect. The excitation signals used in the simulations were acquired by a 0.6-mm-diameter needle hydrophone placed approximately 3 mm from the transducer faces, considering only the plane waves. For the discrete representation method, the emitter aperture, the interface with the defect, and the receiver aperture discretizations ($\Delta x = \Delta y$) were, respectively, 0.15 mm, 0.2mm and 0.2 mm. For all cases, the sampling period was 16 ns.

To give an indication of the approach accuracy, the error respect to the experimental echo response has been calculated for every simulated echo signal in the time domain as:

$$e = \sqrt{\frac{1}{N} \sum_{i=1}^N (s_E(i) - s_C(i))^2} \quad (5)$$

Where $s_E(i)$ is the experimental signal, $s_C(i)$ is the signal computed by the discrete representation method and N the number of samples.

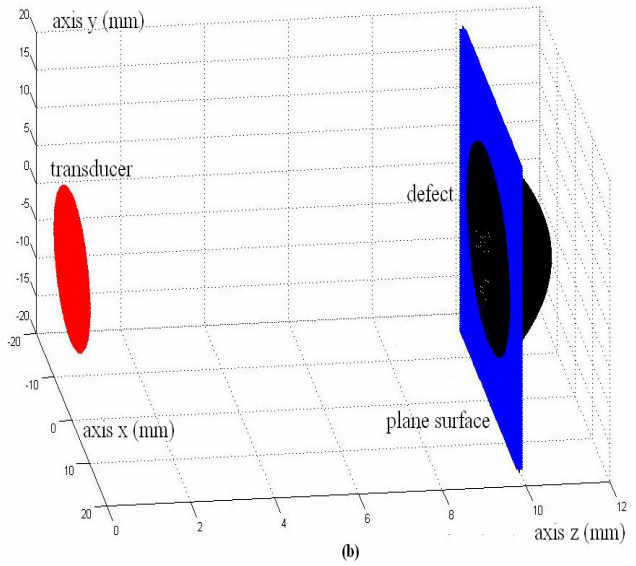
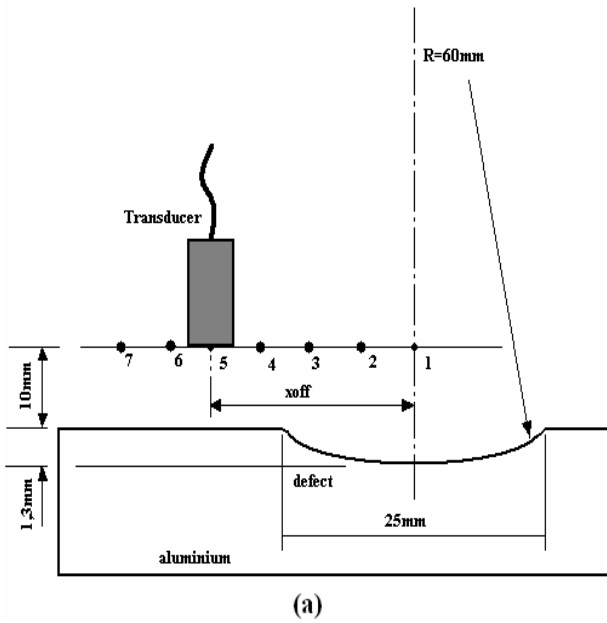


Figure 2. Experimental geometry. (a) Positions 1, 2, 3, 4, 5, 6 and 7 represent, respectively, the transducers displaced 0, 5, 10, 15, 20, 25 and 30 mm from the defect axis; (b) position 7 represented by the 3D model.

The theoretical and experimental results shown in Fig. 3 until 7 were obtained from a 5-MHz transducer with diameter 6.3 mm at positions 7, 4, 3, 2 and 1, respectively. All signals were normalized by the maximum simulated and experimental amplitudes obtained at position 7. For this transducer, the relative errors between the experimental and theoretical echo responses for positions 1, 2, 3, 4 and 7 are, respectively, 12.6%, 3.8%, 1.4%, 11.1% and 16.0%.

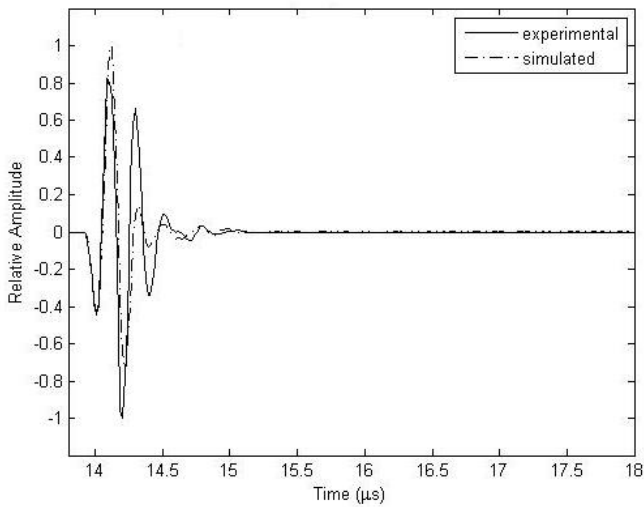


Figure 3. Discrete representation method (dash-dotted line) and experimental (solid line) signals obtained by using the 6.3-mm-diam 5-MHz transducer displaced off the defect axis: (Position 7) 30mm.

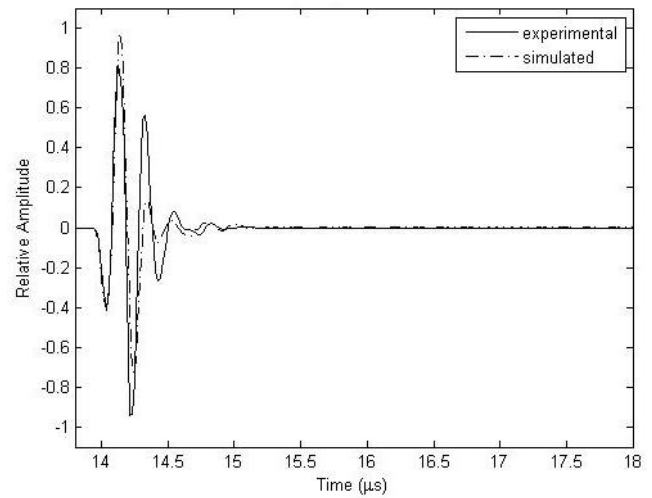


Figure 4. Discrete representation method (dash-dotted line) and experimental (solid line) signals obtained by using the 6.3-mm-diam 5-MHz transducer displaced off the defect axis: (Position 4) 15mm.

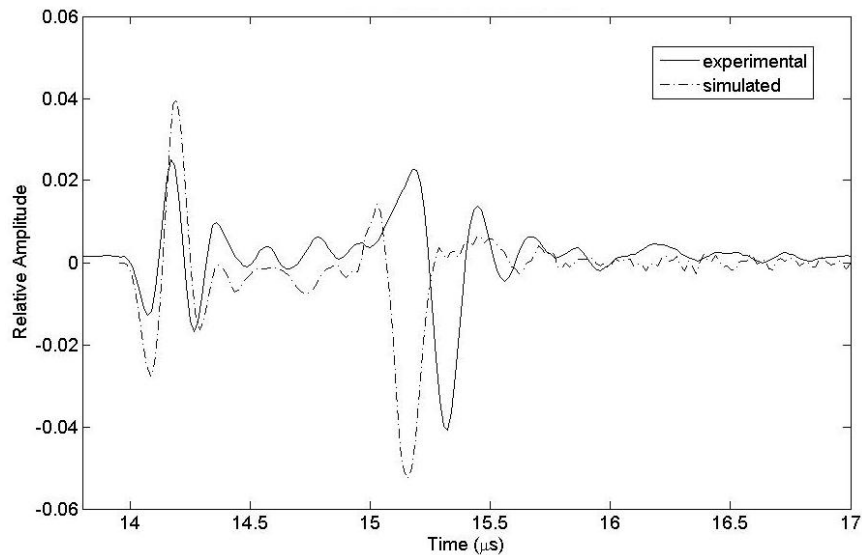


Figure 5. Discrete representation method (dash-dotted line) and experimental (solid line) signals obtained by using the 6.3-mm-diam 5-MHz transducer displaced off the defect axis: (Position 3) 10mm.

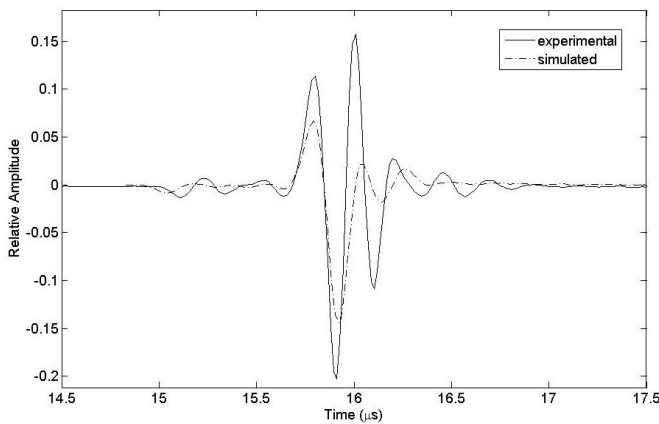


Figure 6. Discrete representation method (dash-dotted line) and experimental (solid line) signals obtained by using the 6.3-mm-diam 5-MHz transducer displaced off the defect axis: (Position 2) 5mm.

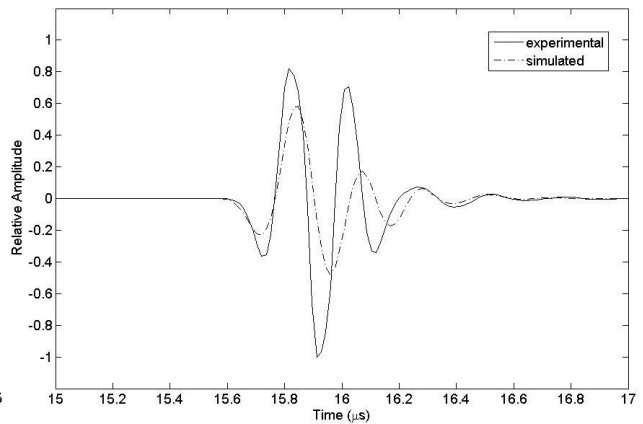


Figure 7. Discrete representation method (dash-dotted line) and experimental (solid line) signals obtained by using the 6.3-mm-diam 5-MHz transducer displaced on the defect axis: (Position 1) 0 mm.

Figures 8, 9 and 10 show comparisons between theoretical and experimental echo responses obtained, from a 19-mm-diam 2.25-MHz transducer, a 10-mm-diam 5-MHz transducer, and a 19-mm-diam 5-MHz transducer, at four different positions.

These transducers were displaced off the defect axis: 0mm (Fig. 8(a), Fig. 9(a), Fig. 12(a)), 5mm (Fig. 8(b), Fig. 9(b), Fig. 10(b)), 10mm (Fig. 8(c), Fig. 9(c), Fig. 10(c)), and 15mm (Fig. 8(d), Fig. 9(d), Fig. 10(d)). All echoes were normalized by the maximum simulated and experimental amplitudes, using the 6.3-mm-diam 5-MHz transducer at position 7 (Fig. 2).

In all cases, the relative errors between the experimental and theoretical echo responses for positions 1, 2, 3 and 4 are, respectively: 18.8%, 3.8%, 1.4% and 11.1% for figure 8; 7.4%, 3.0%, 2.4% and 7.6% for figure 9; and 2.7%, 3.6%, 12.9% and 12.5% for figure 10.

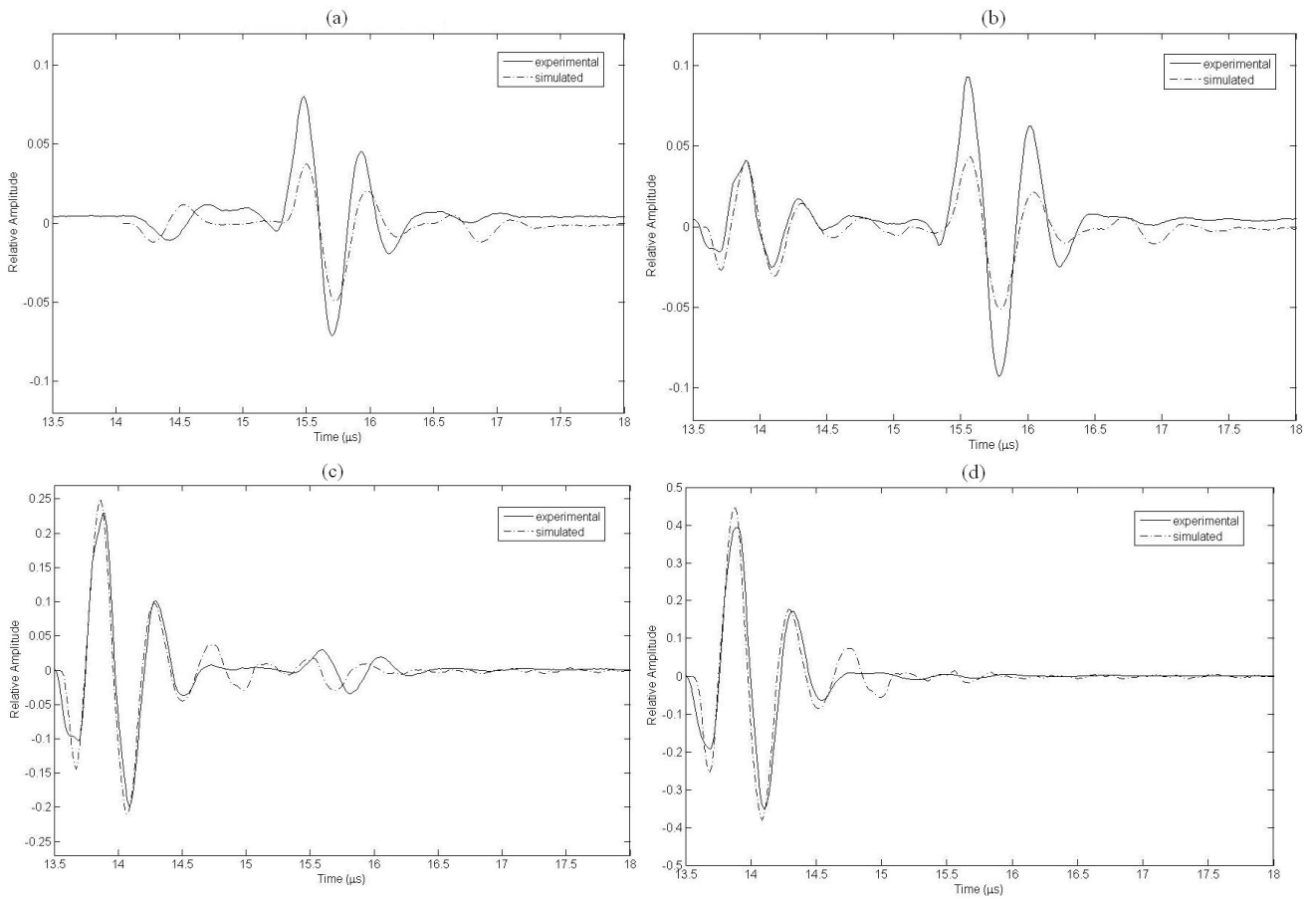
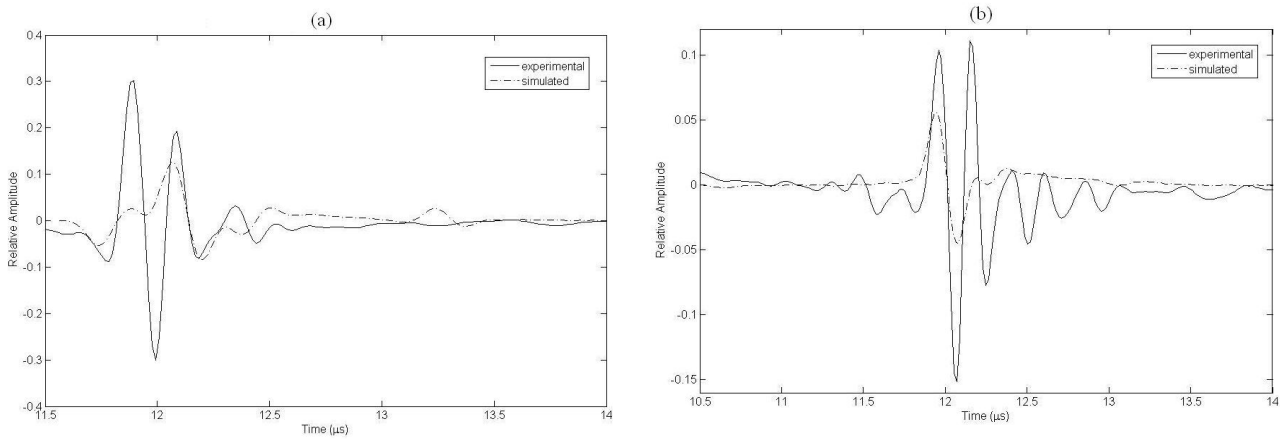


Figure 8. Discrete representation method (dash-dotted lines) and experimental (solid lines) signals obtained by using the 19-mm-diam 2.25-MHz transducer displaced off the defect axis: (a) position 1 = 0mm, (b) position 2 = 5mm, (c) position 3 = 10mm, and (d) position 4 = 15mm.



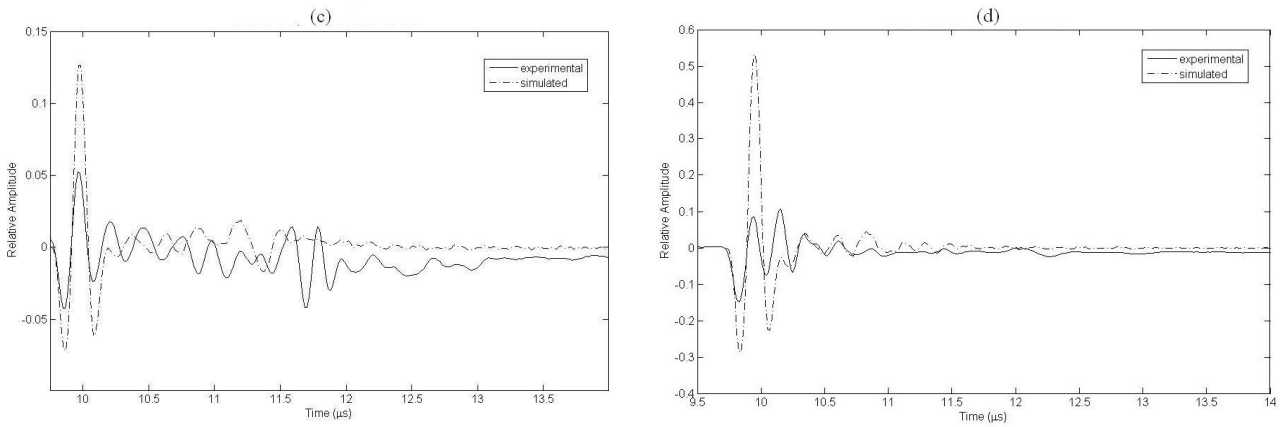


Figure 9. Discrete representation method (dash-dot line) and experimental (solid lines) signals obtained by using the 10-mm-diam 5-MHz transducer displaced off the defect axis: (a) position 1 = 0mm, (b) position 2 = 5mm, (c) position 3 = 10mm, and (d) position 4 = 15mm.

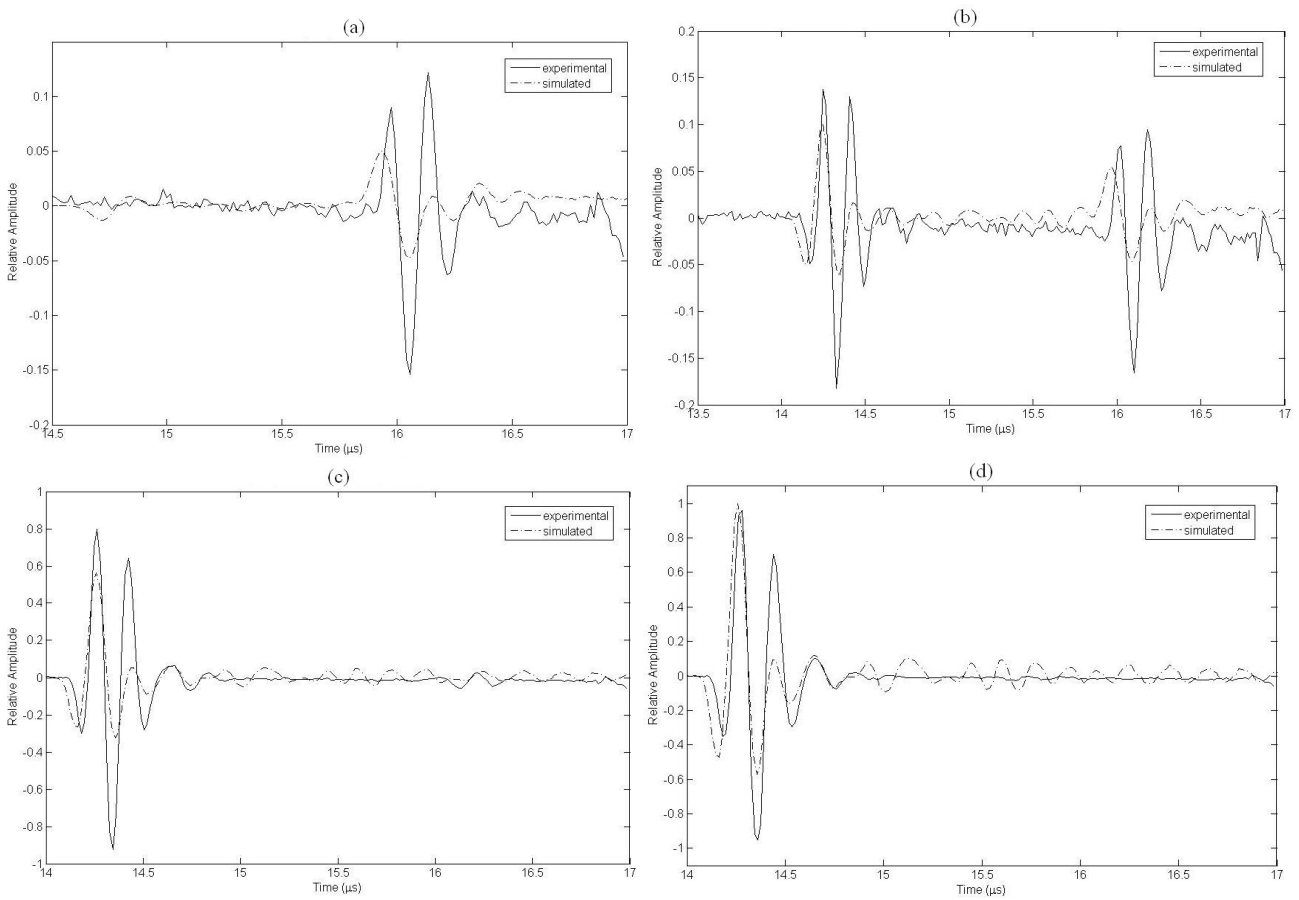


Figure 10. Discrete representation method (dash-dot line) and experimental (solid lines) signals obtained by using the 19-mm-diam 5-MHz transducer displaced off the defect axis: (a) position 1 = 0mm, (b) position 2 = 5mm, (c) position 3 = 10mm, and (d) position 4 = 15mm.

For instance, using a 2.4-GHz Intel Core 2 Duo computer, the processing time for the discrete representation method takes some hours (2-12h, depending on the discretization). Table 1 shows processing times for positions 1, 2, 3 and 4, using four different transducers, considering discretization $\Delta x = 0.2\text{mm}$. Table 2 shows the computational times in position 1 (center of the defect) for four discretization 0.4mm, 0.6mm, 0.8mm, and 1.0mm, using the same transducers shown in table 1.

Table 1: Computational time for each transducer in positions 1 to 4.

Transducers		Computational time (minute)			
Frequency	Diameter	Position 1	Position 2	Position 3	Position 4
2.25MHz	19mm	145.1	210.3	264.4	317.6
5MHz	19mm	142.5	202.6	313.1	331.5
5MHz	10mm	32.9	44.1	53.0	72.4
5MHz	6.3mm	13.7	15.9	26.3	34.2

Table 2: Computational time for each transducer varying the discretization Δx .

Transducers		Computational time (minute)			
Frequency	Diameter	$\Delta x=0.4\text{mm}$	$\Delta x=0.6\text{mm}$	$\Delta x=0.8\text{mm}$	$\Delta x=1.0\text{mm}$
2.25MHz	19mm	34.0 min	14.5 min	9.0 min	5.9 min
5MHz	19mm	35.5 min	15.6 min	9.6 min	6.5 min
5MHz	10mm	8.4 min	3.8 min	2.7 min	1.6 min
5MHz	6.3mm	3.6 min	1.6 min	1.0 min	0.7 min

3.1. Discretization

The accuracy of the discrete representation method depends on spatial and temporal samplings (Buiocchi et al, 2004). The greater the spatial discretization Δx , the more the simulation approaches the exact impulse response method solution (Piwakowski and Sbai, 1999). Moreover, greater temporal discretization leads to better resolution. In this work the temporal discretization was kept at 16ns. Since the computational time increases with the discretizations, a balance between the best samplings and the computational time should be found.

Figure 11 shows the relative errors obtained with the ratio $\Delta x/\lambda$ of 0.30, 0.68, 0.91, 1.22 and 1.35, using the same four transducers placed in position 1 (center of the defect). It indicates that the relative error increases as the discretization of both the transducer and the defect surface decreases. Figure 12 shows the discrete representation method and experimental echoes obtained by using the 2.25-MHz transducer placed in position 7, where in (a) $\Delta x/\lambda = 0.68$, (b) $\Delta x/\lambda = 0.91$, (c) $\Delta x/\lambda = 1.22$, and (d) $\Delta x/\lambda = 1.52$. There is a large deviation between the simulated and experimental results for $\Delta x/\lambda$ greater than 0.91. The small phase difference between simulated and experimental waveforms is due to the imprecision in the propagation velocity obtained from the water temperature measurement and used in the simulation, and the difficulty to experimentally adjust the parallelism between the plane interface and the transducer.

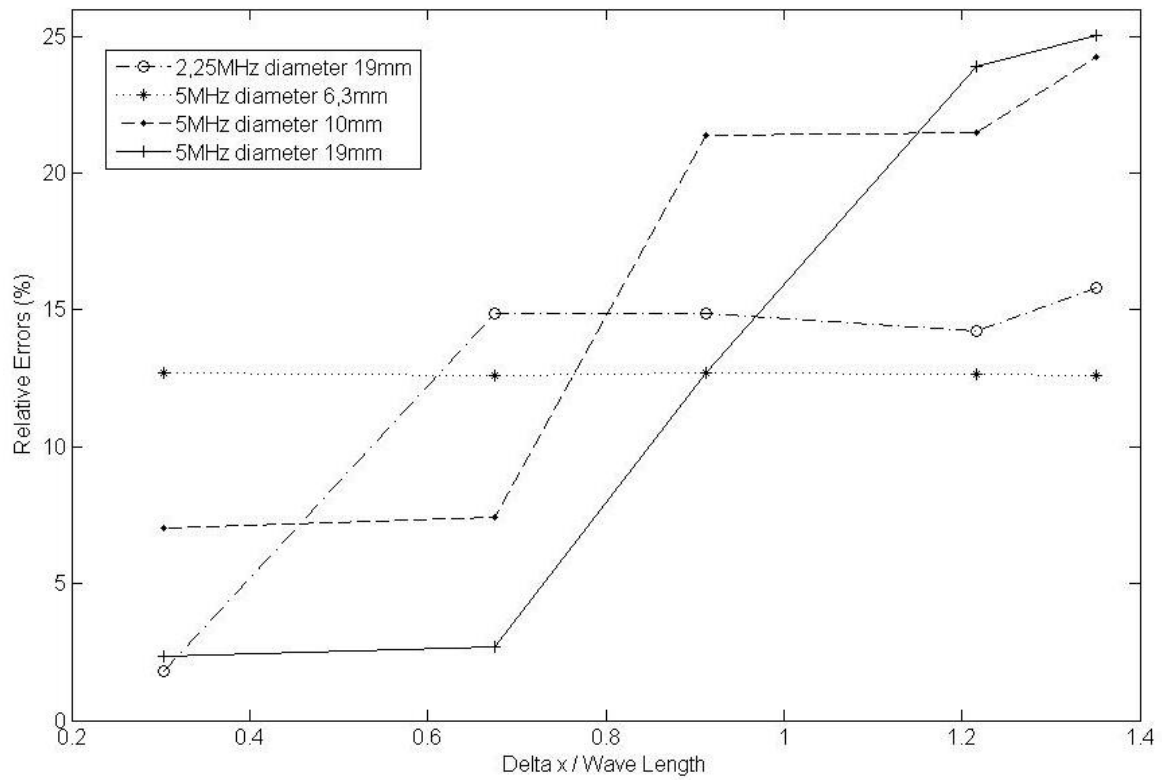


Figure 11: Relative errors with ratio $\Delta x/\lambda$ of 0.30, 0.68, 0.91, 1.22, 1.35.

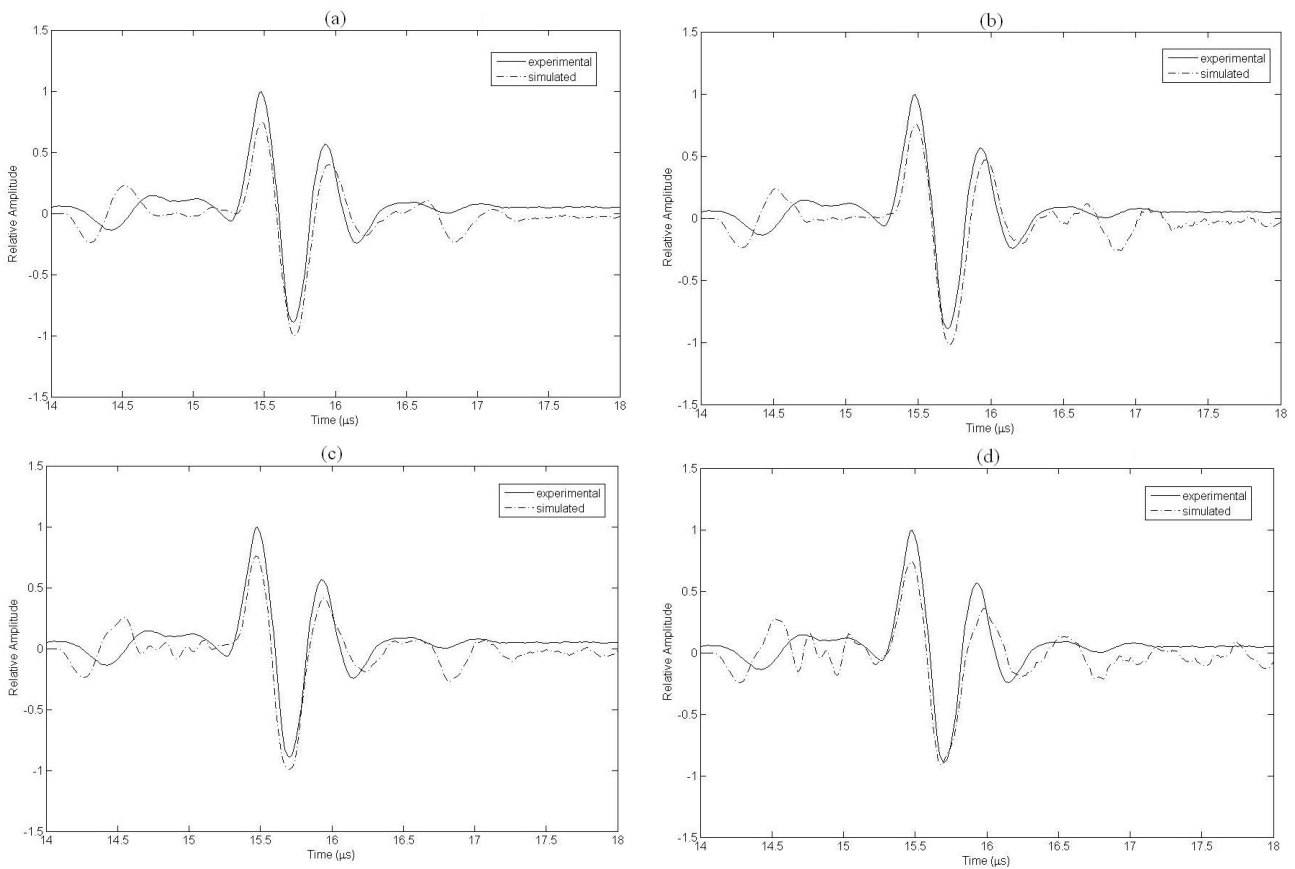


Figure 12: Discrete representation method (dash-dotted lines) and experimental (solid lines) signals obtained by using the 2.25 MHz transducer in position 7: (a) $\Delta x/\lambda = 0.68$, (b) $\Delta x/\lambda = 0.91$, (c) $\Delta x/\lambda = 1.22$, and (d) $\Delta x/\lambda = 1.52$.

4. CONCLUSION

By using three 5-MHz transducers with diameters of 6.3, 10 and 19 mm and a 19mm-diam 2.25MHz transducer, and considering a Δx of 0.2mm and a slightly curved surface of the defect, a good correlation between experimental and theoretical pressure responses from a concave circular defect was shown. The difference of the experimental and theoretical results can be minimized by means of an adequate choice of the ratio between the discretization and wavelength ($\Delta x / \lambda$). An acceptable relative error value is a 15% for $\Delta x / \lambda = 0.68$.

The discrete representation method can be easily extended to arbitrary reflectors with complex geometry defects to predict the echo responses. The knowledge of the pressure response simulated for a given geometry allows accurate interpretations of the echoes generated from corrosions in a realistic pipeline inspection. It provides good understanding of the spatial points where the transducers start and end traveling across the defect.

5. ACKNOWLEDGEMENTS

The authors thank the Brazilian government institutions Petrobras / ANP, FAPESP, and CNPq for the financial support that made this work possible.

6. REFERENCES

- Buiocchi, F., Martínez, O., Ullate, L. G. and Espinosa, F. M. de, "A computational method to calculate the longitudinal wave evolution caused by interfaces between isotropic media", IEEE Trans. Ultrason., Ferroelect., and Freq. Contr. Vol. 51, n. 2, pp. 181-192, 2004.
- Harris, G. R., "Transient field of a baffled planar piston having an arbitrary vibration amplitude distribution," J. Acoust.Soc.Am.,vol.70,pp.186-204, 1981.
- McLaren, S., Weight, J. P., "Transmit-receive mode response from finite-sized targets in fluid media", J. Acoust. Soc. Am., vol. 82, n. 6, pp. 2102-2112, 1987.
- Piwakowski, B. and Delannoy, B., "Method for computing spatial pulse response: Time-domain approach", J. Acoust. Soc. Am., vol. 86, n. 6, pp. 2422-2432, 1989.
- Piwakowski, B. and Sbai, K., "A new approach to calculate the field radiated from arbitrarily structured transducer arrays", IEEE Trans. Ultrason., Ferroelect., and Freq. Contr., vol. 46, n. 2, pp. 422-440, 1999.
- Robinson, D. E., Lees, S. and Bess, L., "Near field transient radiation patterns for circular pistons," IEEE Trans. Acoust., Speech and Signal Processing, vol. 22, n. 6, pp. 395-403, 1974.
- Stepanishen, P. R., "Transient radiation from piston in an infinite planar baffle", J. Acoust. Soc. Am., vol. 49, pp.1629-1638, 1971.
- Weight, J.P., "Ultrasonic beam structures in fluid media", J. Acoust. Soc. Am., vol. 76, pp. 1184-1191, 1984.

7. RESPONSIBILITY NOTICE

The authors are the only responsible for the printed material included in this paper.